BULLETIN OF THE POLISH ACADEMY OF SCIENCES
TECHNICAL SCIENCES, Vol. 58, No. 1, 2010
DOI: 10.2478/v10175-010-0003-9

Vision localization system for mobile robot with velocities and acceleration estimator

P. DUTKIEWICZ*, M. KIEŁCZEWSKI, K. KOZŁOWSKI, and D. PAZDERSKI

Chair of Control and Systems Engineering, Poznan University of Technology, 3a Piotrowo St., 60-965 Poznan, Poland

Abstract. The paper presents a localization system for a mobile robot using the vision system and LED markers and considers the problem of velocity and acceleration estimation in the case of planar motions. Theoretical considerations include the principle of measurement and the details of Kalman estimator with illustrations based on experimental setup. The presented measurement system can be used for a realization of advanced control algorithms for skid-steering mobile robots where significant slippage phenomenon appears.

Key words: vision localization system, mobile robot, acceleration estimator.

1. Introduction

A localization of mobile robots, namely the determination of their current position and orientation in a configuration space, becomes a fundamental problem to be solved for the proper realization of control and navigation tasks [1, 2]. Considering different localization approaches one can distinguish relative and absolute solutions. The relative methods, such as the odometry or inertial localization, are based on onboard sensors including shaft-encoders, accelerometers or gyros which measure internal state of the robot and are not directly influenced by an environment [3]. Thus, the current configuration has to be estimated using integration methods that makes the results to be relative and prone to parameter and structural uncertainties. Otherwise, one can use absolute localization techniques such as triangulation, vision processing, etc., which use exterior sensors interacting with an environment (i.e. laser and ultrasonic rangefinders, radio devices, cameras, etc.) [4, 5]. However, absolute methods may provide less accurate results affected by significant delay due to sensor limitations or high computational costs. Therefore, one can consider a combination of the above methods as a good solutions [6].

The requirements of high accuracy and low-time delay with respect to the localization systems become critical when they are used in the control feedback. In particular, an advanced control algorithms designed for underactuated mobile robots in order to realize basic motion tasks (i.e. regulation, path following and trajectory tracking) impose high demands on a sensor system [7]. This issue is reported, for example, by Dixon et al. [8] concerning a vision system which can significantly limit the overall control performance. Moreover, considering robots dynamics usually one has to measure or estimate velocities or even accelerations of the robot. For wheeled robots this issue is especially crucial in the case, when significant skid-slip phenomenon appears between the wheels and the surface on which they move [9]. Then determining of the robot velocity based only on simple geometric relationships is no longer possible. Instead of that one can use onboard sensors set for velocity measurements in the local coordinate system, or use exterior measurement system to estimate velocity and acceleration in the global coordinate system.

In this paper it is shown that the localization based on a vision system may satisfy high accuracy and low time-delay requirements. Using Kalman filter it is possible to obtain velocities and accelerations without any additional set of sensors with quality sufficient for advanced control algorithms realization. In comparison to previous works [7, 10] where analog PAL camera is used, the performance of the proposed vision localization system is significantly improved. It is achieved using the hardware based on a digital camera with the progressive scan CCD sensor working with frequency up to 64 frames per second. The accuracy improvement is assured using a new image processing algorithm which gives possibility to dramatically increase measurement resolution (even by two order of magnitude with comparison with the classical methods). According to the best authors' knowledge the overall system is a new solution and a similar localization system so far has never been addressed in the automation and robotics literature.

The paper is organized as follows. In Sec. 2 the proposed vision localization system is presented. The description includes design assumptions, the system structure, principle of image acquisition and processing based on a new convolution-like algorithm. The principle of position and orientation measurement using a marker along with error analysis are discussed. Third Sec. is devoted to the observer design based on the Kalman filter. The next Sec. describes experimental results. To show an effectiveness of velocity estimation an application of slip compensation with respect to the skid-steering robot is shown. Last Sec. is devoted to the concluding remarks.

2. Localization system

2.1. Preliminary design assumptions. A localization system considered here is designed in order to determine the config-

*e-mail: Piotr.Dutkiewicz@put.poznan.pl

uration of robot's body in a case of planar motion. Assume that the configuration of the robot moving on a plane (see Fig. 1) is described as follows

$$\boldsymbol{q} = [\theta \ \boldsymbol{p}^T]^T \in \mathbb{S}^1 \times \mathbb{Q}_p, \tag{1}$$

where $\mathbb{Q}_p \subset \mathbb{R}^2$, angle θ denotes orientation of the local coordinate frame $x_l y_l$ with respect to the inertial coordinate frame $X_g Y_g$ and $\boldsymbol{p} = [X \ Y]^T \in \mathbb{Q}_p$ determines the origin of the local frame. It is assumed that the designed measurement system should provide velocities and accelerations expressed in the local coordinate frame. In order to meet this assumption the following velocity transformation is applied

$$\dot{\boldsymbol{q}} = \boldsymbol{\Theta}(\theta)\, \boldsymbol{v}, \tag{2}$$

where $\boldsymbol{\Theta}(\theta) = \left[\begin{smallmatrix} 1 & \boldsymbol{0} \\ \boldsymbol{0} & \boldsymbol{R}(\theta) \end{smallmatrix}\right]$, and $\boldsymbol{R}(\theta) \in \mathrm{SO}(2)$ is a rotation matrix and vector $\boldsymbol{v} = [\omega \ v_x \ v_y]^T \in \mathbb{R}^3$ describes angular velocity and linear velocity components given in the local coordinate frame.

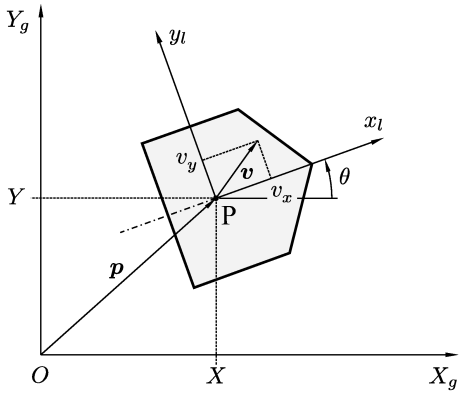

Fig. 1. Free body kinematics for unconstrained plane motion

It is supposed that the output of the measurement system is represented by the 9-element vector of selected quantities

$$\boldsymbol{y} = \begin{bmatrix} \boldsymbol{q}^T & \boldsymbol{v}^T & \boldsymbol{a}^T \end{bmatrix}^T \in \mathbb{S}^1 \times \mathbb{Q}_p \times \mathbb{R}^6, \tag{3}$$

with acceleration vector $\boldsymbol{a} = \dot{\boldsymbol{v}}$.

2.2. General description of localization system structure. The localization system shown in Fig. 2 consists of a camera, a marker, PC computer with an image acquisition card and dedicated application. The camera is fixed above the scene surface at 3 m and gives possibility to observe rectangle area with dimensions 2.2×1.6 m where the marker with LED diodes is placed. The position and orientation of the marker is calculated based on the diodes image. The VISTEK SVS 084MSCL digital black and white camera combined with the PENTAX H612A (focal length 6 mm) lens is used. It is based on the progressive scan 1/3″ CCD sensor with effective resolution 658×494 pixels and maximum image acquisition frequency 64 frames per second. Image acquisition from the camera to PC computer memory is performed by the Euresys GrabLink Value PCI framegrabber card. The camera is connected to the acquisition card via the digital interface CameraLink.

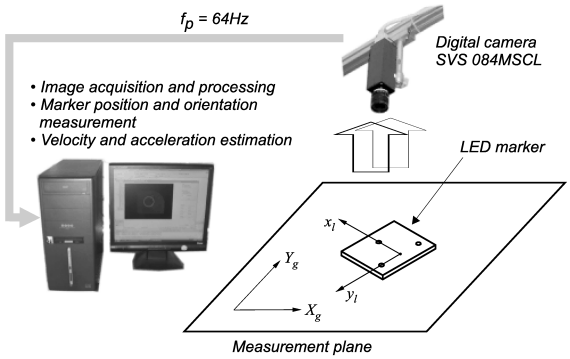

Fig. 2. Structure of the vision localization system

The marker consists of a plate with three LED diodes which constitute rectangular isosceles triangle. In order to improve robustness of the vision system to external non stationary lighting conditions, high brightness LED diodes are used. Moreover, it gives possibility to significantly shorten exposure time of the camera in order to remove additional blur of the diodes, resulting from the fast marker motion.

The PC computer equipped with the Athlon 64 X2 3800+ processor works under the Windows XP operating system. The application was built based on the Microsoft Visual C++ 6.0 development platform supported by the MultiCam library for image acquisition using the Euresys framegrabber card. The main tasks of the application are position and orientation measurements, velocity and acceleration estimation, and finally implementation of the proposed system in the closed loop.

2.3. Principle of image processing. The vision localization system uses marker composed of LED diodes. The single measurement uses an image from the camera which is processed in order to determine position of the LEDs on the image. Following that, points which represent centers of LEDs are transformed from the image coordinate space to the physical coordinates expressed in the global coordinate frame.

In order to use the vision system as an accurate measurement system, proper calibration of the camera is necessary. To realize that usually two coordinates frames are used, namely the external reference frame and the internal camera frame. During the calibration procedure projection parameters are determined, which are commonly divided into the geometric (extrinsic) parameters and optical (intrinsic) parameters directly related to the camera [11, 12]. Extrinsic parameters describe position and orientation of the camera frame with respect to the global reference frame. They are determined from the translation and rotation matrix which can be represented in terms of the three Euler angles. Intrinsic camera parameters consist of a focal length, the principal point describing a position of the optical axis projection into the image space, the skew coefficient described as an angle between image axes and the distortion vector which includes radial and tangential distortion coefficients.

The calibration was done in the Matlab environment using the Camera Calibration Toolbox [13] which is based on

22 images with the chessboard-like pattern placed in different configurations. It was assumed that tangential and the second and the fourth order radial distortions are taken into account for the used camera model. Besides distortion parameters, during the calibration procedure, the principal point, the focal length and the skew coefficient were estimated. All these parameters are used in the reprojection procedure from the image coordinate space to the Cartesian coordinate frame.

In order to achieve the effective frequency of the localization system and the optional control loop equal to 64 Hz, the triple buffering method of image acquisition is used. It gives possibility for simultaneous image acquisition while image in the other buffer is being processed. Apart from an appropriate image acquisition technique, the performance of the image processing algorithm is essential and the average processing time should not exceeded a period of the single image acquisition from the camera.

At the first stage of the image processing the following steps are realized: logical filtering, binarization, finding connected group of pixels, recognizing three groups which constitute triangle of the marker, determining centers of three blobs representing diodes and calculating position and orientation. The first three steps are combined during the single pass of an image buffer processing. To find a bright group of pixels representing diodes, consecutive pixels of the image are compared with the brightness threshold and with the fixed neighborhood pixels. If pixel passes the logical filter condition, from this point procedure of finding the connected group of pixels (ie. blob) is started and its result is stored in the auxiliary binary image. For all found blobs their centers are determined as an arithmetic average of the pixels coordinates. Then based on geometrical relationships between obtained center points triangle of the marker diodes is found – see Fig. 3.

Fig. 3. Negative of the LED blobs in the image

Considering design requirements formulated for the localization system the spatial resolution, restricted to one pixel, becomes highly not satisfactory. Hence at the second stage of processing an effective algorithm which significantly decreases size of space quantization step based on luminance image of each diode is proposed. From Fig. 3 one can see that an image of each diode is blurred significantly in spite of its small lighting area which should be contained in just one pixel. For the proposed algorithm it is assumed that diodes can be considered as light sources and their blurred image is a consequence of low-pass filtering due to light disperse which comes from optics aberrations and antialiasing filter[1]. Hence, the image projected onto the camera sensor can be regarded as a result of continuous two dimensional convolution of small spot light intensity function and low-pass unknown filter operator. For the considered algorithm the parametric description of the low-pass filter impulse response is assumed (alternatively one can use a nonparametric approach discussed for example in [14]) in the form of the Gauss two-dimensional function. It was observed that such approximation gives quite accurately convolution results which well correspond to the image projected on the camera sensor.

Next the camera sensor performs two-dimensional discretization of the continuous image. Accordingly one can search for the point light source considering the continuous luminance function defined on the sensor area. It can be realized using the deconvolution operation in order to eliminate the sampling operator and the Gauss filter operator.

Since the luminance signal provides very important information one should be aware that the described algorithm may provide good results only if the blurred diode image is properly quantized with respect to the dynamic range of camera sensor. Especially sensor saturation should be avoided which can be guaranteed by proper selection of the amplifier gain, the lens aperture and shutter speed. In addition, one has to take into account that the blur motion should be limited. Hence, exposure time should be set small enough with respect to the expecting range of the marker velocity.

In order to determine position of the light source with high precision first, one should find the pixel where center of the source is placed. This can be realized by searching the pixel for which neighborhood pixels[2] carry maximum energy which represents the most probability of the light source center position. Next, dividing this pixel into $m \times m$ parts (which means that each side of it is divided into m parts) one can perform the numerical deconvolution with high resolution. As a result, the position of the diodes center can be determined with m-higher precision in each direction. For the implemented version of the algorithm 5×5 neighborhood is used and $m = 100$.

2.4. Position and orientation measurement. Now we assume that the position of three LEDs, placed at points P_1, P_2 and P_3 (see Fig. 4) are represented in the inertial frame by vectors $\boldsymbol{p}_1$, $\boldsymbol{p}_2$ and $\boldsymbol{p}_3$.

Then one can calculate the configuration of the marker as follows

$$\boldsymbol{p} = \frac{1}{2}\left(\boldsymbol{p}_1 + \boldsymbol{p}_2\right) \tag{4}$$

and

$$\theta = \operatorname{atan2}\left(d_y, d_x\right) + \alpha, \tag{5}$$

[1]In fact such assumption also covers the effect that for a real diode, the light is emitted by non zero area.

[2]The initial position is determined taking into account the results from the first stage of the image processing.

where d_x and d_y represent coordinates of vector $\boldsymbol{d}$ given by

$$\boldsymbol{d} = \boldsymbol{p} - \boldsymbol{p}_3 = \frac{1}{2}(\boldsymbol{p}_1 + \boldsymbol{p}_2) - \boldsymbol{p}_3, \tag{6}$$

where α is equal to 180 degrees according to Fig. 2.

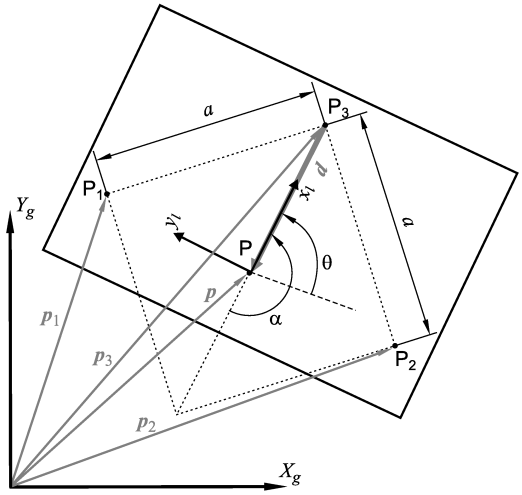

Fig. 4. Marker using three LEDs in the inertial frame

Considering accuracy of the measurement method it is assumed that maximum error of determination of each component of vectors $\boldsymbol{p}_i$, where $i = 1, 2, 3$ in the inertial frame on the operational area does not exceed ϵ. Calculating the total differential with respect to Eqs. (4) and (5) one can estimate the maximum position and orientation measurement error as follows

$$|\Delta X|, |\Delta Y| \leq \epsilon \Rightarrow \|\Delta \boldsymbol{p}\| \leq \sqrt{2}\epsilon \tag{7}$$

and

$$|\Delta\theta| \leq \frac{2\epsilon}{\|\boldsymbol{d}\|}\left(|\sin(\theta-\alpha)| + |\cos(\theta-\alpha)|\right). \tag{8}$$

or using more conservative bound

$$|\Delta\theta| \leq \frac{4\epsilon}{a}, \tag{9}$$

where a denotes the geometric base indicated by length of two sided of isosceles triangle – see Fig. 4. According to result (9) increasing base a results in the better orientation accuracy measurement. This obvious implication limits the minimum size of the marker.

3. Observer design based on Kalman filter

First suppose that the localization system provides the current real configuration $\boldsymbol{q}$ of the marker (placed on the robot's body) at each time instant. Moreover, it is assumed that $\boldsymbol{q}$ is not affected by the quantization noise. Then in order to estimate its velocities one can calculate the difference quotient of the configuration as follows

$$\dot{\boldsymbol{q}} \approx \frac{1}{T_s}(\boldsymbol{q}_n - \boldsymbol{q}_{n-1}), \tag{10}$$

where T_s denotes sampling time and n determines the number of samples. In practice using so called difference estimator can be inefficient since it is extremely prone to the measurement noise. Consider now that signal $\boldsymbol{q}^*$, provided by the localization system, is significantly affected by uncertainty term $\delta\boldsymbol{q}$ such that

$$\boldsymbol{q}^* \triangleq \boldsymbol{q} + \delta\boldsymbol{q}, \tag{11}$$

where $\boldsymbol{q}$ is the real but unknown configuration. Then one can easily prove that using the estimator given by Eq. (10) multiplies the standard deviation of noise by the factor $1/T_s$. The term $\delta\boldsymbol{q}$ is a direct consequence of quantization noise and includes high frequency components in its spectrum. As a result the velocity estimation may lead a low signal to the noise separation especially in the case of slow motions. Following this observation, it is clear that the estimation of accelerations based on this method becomes almost useless (the noise will be amplified $1/(T_s)^2$ times).

In order to improve robustness to noise the low-pass filtering can be used since the noise energy is mostly located in the high frequency spectrum range. This technique can be used effectively only if the sampling frequency is high enough with respect to the required bandwidth. In this case the significant oversampling is needed in order to decrease a phase lag introduced by the low-pass filter which may be critical for the control realization in the closed-loop because of the stability issue. Such requirement may be difficult to satisfy as a result of a limited camera performance and a cost increase.

The other estimation techniques include, for example, robust sliding non-smooth methods proposed by Levant [15], Kalman filters [16], particle filtering, etc. Taking into account that the considered process model can be described with a satisfactory accuracy, the extended Kalman algorithm (EKF) was chosen to estimate velocity and acceleration.

In the considered case, it is assumed that the input signal $\boldsymbol{q}^*$ is obtained by the localization system and measurement noise indicated by $\delta\boldsymbol{q}$ is a vector of random variables with mean zero values and statistical properties characterized by the measurement covariance matrix $\boldsymbol{Q}_R \in \mathbb{R}^{3\times3}$.

The suitable process modeling is a key for the proper estimation, using the Kalman filter. It is assumed that sampling time T_s is small with respect to the dynamics of considered motion and the Euler forward integration method used for discretization is sufficient.

Extending kinematics (2) by adding process dynamics and applying the numerical integration to the overall system one can obtain the following discrete model of the plane motion

$$\boldsymbol{x}_n = \boldsymbol{f}(\boldsymbol{x}_{n-1}, \boldsymbol{u}_{n-1}) = \boldsymbol{F}(\theta_{n-1})\,\boldsymbol{x}_{n-1} + \boldsymbol{G}\boldsymbol{u}_{n-1}, \tag{12}$$

where $\boldsymbol{x}_n$ denotes the state such that

$$\boldsymbol{x}_n \triangleq \left[\boldsymbol{y}_n^T \;\; \boldsymbol{z}^T\right]^T, \tag{13}$$

$\boldsymbol{y}$ is an output defined by Eq. (3), $\boldsymbol{z} \triangleq \dot{\boldsymbol{a}}$ denotes jerk and

$$\boldsymbol{F}(\theta_{n-1}) \triangleq \begin{bmatrix} \boldsymbol{I}_{3\times3} & T_s\boldsymbol{\Theta}(\theta_{n-1}) & \boldsymbol{0}_{3\times3} & \boldsymbol{0}_{3\times3} \\ \boldsymbol{0}_{3\times3} & \boldsymbol{I}_{3\times3} & T_s\boldsymbol{I}_{3\times3} & \boldsymbol{0}_{3\times3} \\ \boldsymbol{0}_{3\times3} & \boldsymbol{0}_{3\times3} & \boldsymbol{I}_{3\times3} & T_s\boldsymbol{I}_{3\times3} \\ \boldsymbol{0}_{3\times3} & \boldsymbol{0}_{3\times3} & \boldsymbol{0}_{3\times3} & \boldsymbol{I}_{3\times3} \end{bmatrix} \in \mathbb{R}^{12\times12} \tag{14}$$

is the process matrix which depends on orientation θ_{n-1} determined in the previous step, with identity matrix $\boldsymbol{I}_{k\times k} \in \mathbb{R}^{k\times k}$ and zero matrix $\boldsymbol{0}_{k\times k} \in \mathbb{R}^{k\times k}$,

$$\boldsymbol{G} \triangleq \begin{bmatrix} \boldsymbol{0}_{3\times 3} & \boldsymbol{0}_{3\times 3} & \boldsymbol{0}_{3\times 3} & \boldsymbol{I}_{3\times 3} \end{bmatrix}^T \in \mathbb{R}^{12\times 3} \tag{15}$$

is an input matrix and $\boldsymbol{u} \triangleq \dot{\boldsymbol{z}} \in \mathbb{R}^3$ denotes input signal in the form of time derivative of jerk described in the local frame of the marker.

The input signal $\boldsymbol{u}$ is not measured and its value is unknown. Hence, we assume that $\boldsymbol{u}$ can be considered as a vector of random variables. Moreover, in order to include some uncertainties in the model which result from discretization and jitter introduced by small fluctuations of sampling time the process noise is added also to other variables. Summarizing the process noise is modeled as the vector $\boldsymbol{w} \in \mathbb{R}^{12}$, describing noise with the zero mean value, i.e. $E(\boldsymbol{w}) = \boldsymbol{0}$ and process covariance matrix $\boldsymbol{Q}_M \in \mathbb{R}^{12\times 12}$. As a result Eq. (12) can be rewritten into the following form

$$\boldsymbol{x}_n = \overline{\boldsymbol{f}}\left(\boldsymbol{x}_{n-1}, \boldsymbol{w}_{n-1}\right) = \boldsymbol{F}\left(\theta_{n-1}\right)\boldsymbol{x}_{n-1} + \boldsymbol{Q}_M \boldsymbol{w}_{n-1}. \tag{16}$$

It should be emphasized that the most significant difficulty comes from the determination of the covariance matrix $\boldsymbol{Q}_M$. In general in many cases it is chosen based on the trails and errors method [17]. In the considered case one can suppose that matrix $\boldsymbol{Q}_M$ is diagonal such that

$$\boldsymbol{Q}_M \triangleq \operatorname{diag}\left\{\boldsymbol{Q}_{Mq}, \boldsymbol{Q}_{Mv}, \boldsymbol{Q}_{Ma}, \boldsymbol{Q}_{Mz}\right\}, \tag{17}$$

with $\boldsymbol{Q}_{M\xi} \in \mathbb{R}^{3\times 3}$ (for $\xi \in \{q, v, a, z\}$) denoting covariance matrices with respect to coordinates, velocities, accelerations and jerks, respectively. Taking into account that input $\boldsymbol{u}$ is unknown, the matrix $\boldsymbol{Q}_{Mz}$ should have predominant coefficients. Moreover, assuming that the marker is placed on the robot, one can also consider the different dynamics for angle and linear motions during a selection of matrix $\boldsymbol{Q}_{Mz}$.

The reference model, given by Eq. (16), is nonlinear because of nonlinear velocity mapping from the inertial to the local moving frame. In order to cope with nonlinearity one can consider the extended Kalman filter and define linearized reference process as

$$\boldsymbol{x}_n \approx \boldsymbol{A}\boldsymbol{x}_{n-1}, \tag{18}$$

where

$$\boldsymbol{A} \triangleq \left.\frac{\partial \overline{\boldsymbol{f}}}{\partial \boldsymbol{x}_{n-1}}\right|_{\boldsymbol{x}_{n-1}=\widehat{\boldsymbol{x}}_{n-1}}$$

is the Jacobian matrix. According to Eq. (11) the measurement can be described as follows

$$\boldsymbol{q}^* = \boldsymbol{C}\boldsymbol{x} + \delta\boldsymbol{q} \tag{19}$$

where $\boldsymbol{C} \triangleq \left[\boldsymbol{I}_{3\times 3}\ \boldsymbol{0}_{3\times 9}\right]^T \in \mathbb{R}^{3\times 12}$.

The realization of the Kalman recursive algorithm is classical and consists of prediction and next correction substeps. The details can be found for example in [16, 17]. After the realization of one complete step of the EFK algorithm one obtains estimates $\widehat{\boldsymbol{x}}$ and $\widehat{\boldsymbol{y}}_n$ defined by Eq. (3) which contain an estimation of coordinates, velocities and accelerations.

4. Experimental research

4.1. Introduction. The experimental testbed consists of the system described in Subsec. 2.2. Taking into account the resolution of CCD sensor the base relative accuracy is $1/658 \approx 1.52 \cdot 10^{-3}$ and considering coefficient scale one can obtain that one pixel size corresponds to the square area about 3×3 mm.

4.2. Configuration measurement in a static case. During this experiment the marker was fixed to the rotating wheel with axis parallel to the optic axis of the camera presented in Fig. 5. The wheel was used in order to set the desired orientation of the marker from 0 to 90 deg with step 15 deg. Then for each selected marker the steady posture series of 4,000 samples were recorded. For each series the mean value of vector coordinates was calculated and the deviation from the mean value was determined. Considering all data (including 28,000 samples) statistics were examined and normalized histogram illustrating discrete density functions determined for each coordinates were calculated (see Fig. 6). Accordingly, for each random variable the standard deviation was calculated and the corresponding continuous density function based on the Gaussian distribution was plotted. As one can see from Fig. 6 distributions, calculated from the experimental data, are quite different from corresponding Gaussian distributions. In particular some holes in histogram of the data describing position appear due to imperfect deconvolution during the image processing. It is a result of the assumed low-pass filter approximation using the Gaussian function (note that the histogram is affected by $\sin x/x$ function).

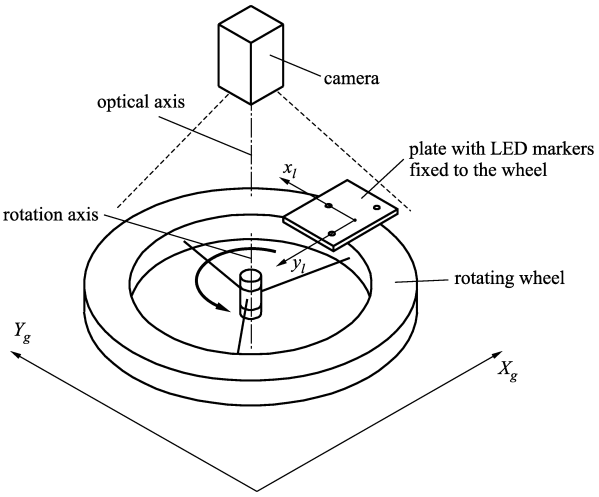

Fig. 5. Experimental setup for static and dynamic accuracy evaluation

According to performed data analysis one can estimate the static local accuracy[3]. The relative position error δ_p is calculated with respect to the width of the CCD sensor and it is independent on the coefficient scale within quite wide range.

[3]The real accuracy in whole coordinate space is obviously worse as a result of non ideal camera calibration.

a) Position deviation in X-axis

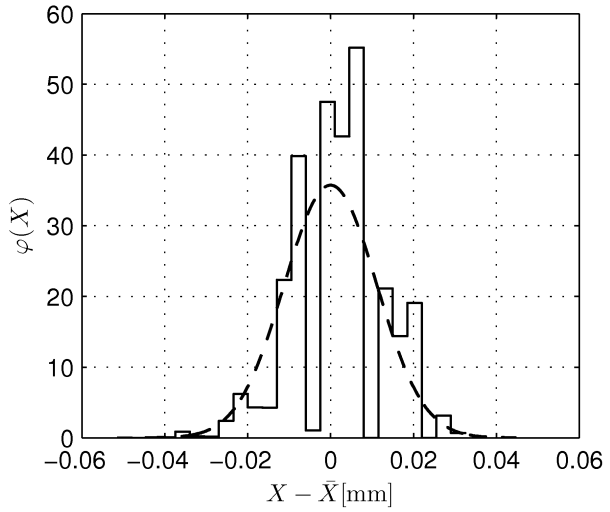

b) Position deviation in Y-axis

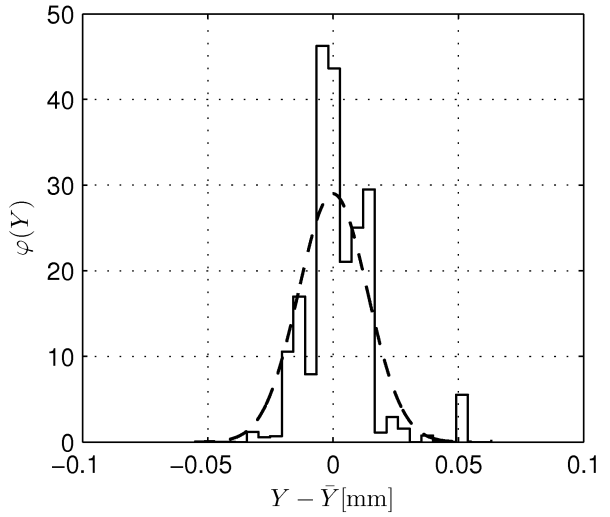

c) Angle deviation

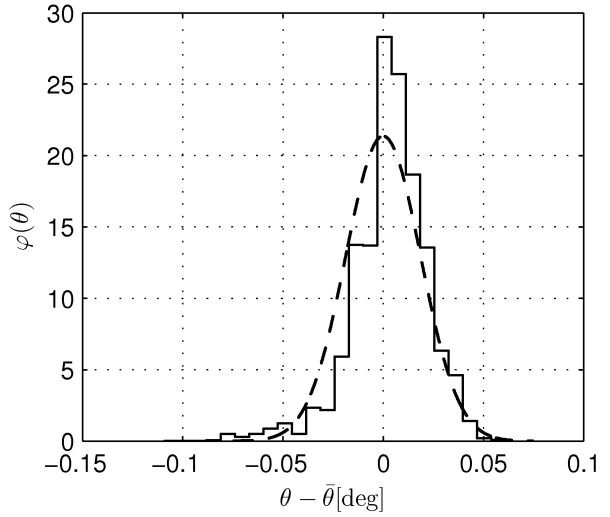

Fig. 6. Probability density functions for static case: histogram (–), corresponding Gaussian function (– –)

The increase of the relative error can be observed for small coefficient scale since image of the LEDs does not correspond to the marker model assumed in the image processing procedure. On the other hand, for the large coefficient scale magnitude of the light intensity function decreases. The relative orientation error is obtained for the particular case of marker and the optical system geometry with respect to the round angle (2π rad). However, it is significantly dependent on the coefficient scale. In order to get quantitative description the following formula is used

$$\delta_\theta\left(\overline{a}\right) \triangleq \frac{1}{\overline{a}}\,\overline{\delta}_\theta, \tag{20}$$

where

$$\overline{a} \triangleq a^{\#}/w^{\#}$$

is relative length with $a^{\#}$ is size of the marker expressed in pixels while $w^{\#}$ is the horizontal resolution (in this case $w^{\#} = 658$), $\overline{\delta}_\theta$ is normalized relative orientation error determined as follows

$$\overline{\delta}_\theta \triangleq \overline{a}_0\delta_\theta \approx 1.9 \cdot 10^{-5}, \tag{21}$$

where

$$\overline{a}_0 = \frac{43}{658} \quad \text{and} \quad \delta_\theta = 2.8 \cdot 10^{-4}$$

are determined based on experimental results.

Comparing results given in Table 1 one can conclude that the subpixel resolution allows to increase the accuracy 60 times with respect to the standard pixel case. From theoretical considerations it follows that the increase should be even higher and should reach 100 (each pixel is divided into 100×100 parts) but it is limited due to the simplification in the algorithm and some unmodeled phenomena.

Table 1
Absolute and relative local accuracy in the static case

Absolute position error	$\Delta_p < 0.05$ mm
Absolute orientation error	$\Delta_\theta < 0.1$ deg
Relative position error	$\delta_p < 2.3 \cdot 10^{-5}$
Relative orientation error	$\delta_\theta < 2.8 \cdot 10^{-4}$

4.3. Configuration measurement in a dynamic case. The experimental setup used for the dynamic case is the same as in the static case. Initially the wheel with fixed marker was set rotated by hand and next the marker motion was recorded with sample time $T_s = 1/64$ s. The angular velocity of the wheel slowly decreased as a result of a resistive torque appearing in the wheel bearing.

Taking into the account the error analysis it was assumed that the noise signal mostly occupies the higher part of frequency spectrum. In turn, the useful signal related to the marker motion are located within the low frequency range. Hence, one can separate noise signal using the high-pass filtering. In the considered case the high-pass 10th order discrete Butterworth filter with cut-off frequency $f_c = 0.05/T_s = 3.2$ Hz was used. The high-pass filtered coordinates are denoted as θ^f, X^f, and Y^f.

a) Position deviation in X-axis

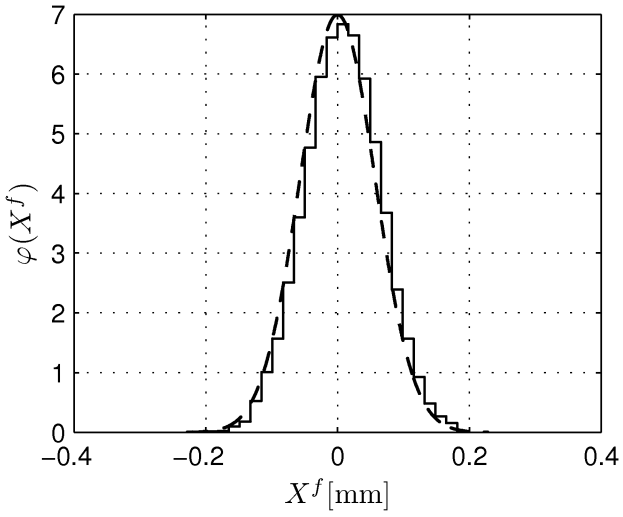

b) Position deviation in Y-axis

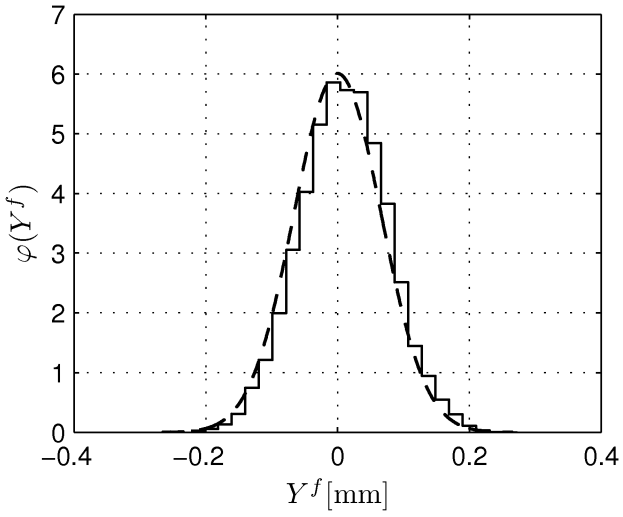

c) Angle error

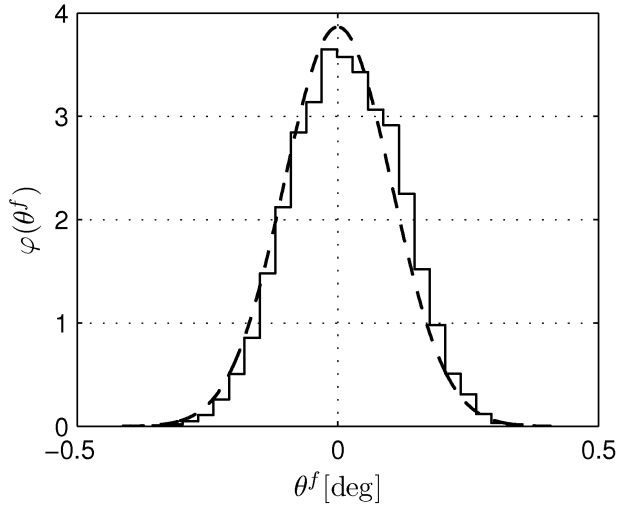

Fig. 7. Probability density functions for dynamic case: histogram (–), corresponding Gaussian function (– –)

In Fig. 7 discrete density functions determined for the filtered coordinate signals with corresponding Gaussian distributions are shown. As one can see each coordinate statistics distribution of the measured data is quite similar to the normal distribution. The standard deviations were increased with respect to ones obtained for static case about 4 times. Moreover, it was observed that the accuracy in the dynamic case is almost the same within quite high range of the marker velocity (however different from zero). The worse accuracy in the dynamic case comes from the camera clock phase changing, namely jitter and other phenomena related to CCD matrix properties.

From the measurement data the covariance matrix $\boldsymbol{Q}_R$ was calculated and next it was used as a parameter of the EKF algorithm. The covariance matrix $\boldsymbol{Q}_M$ was chosen based on the trials and errors method according to the observations of filtering results. Finally, it was assumed that $\boldsymbol{Q}_q = \boldsymbol{Q}_v = \boldsymbol{Q}_a = \boldsymbol{0}_{3\times 3}$ and $\boldsymbol{Q}_z = \mathrm{diag}\{10, 0.1, 0.1\} \cdot T_s$. In Fig. 9 and Fig. 8 the results of estimation using two alternative method

a) Estimates for higher velocity

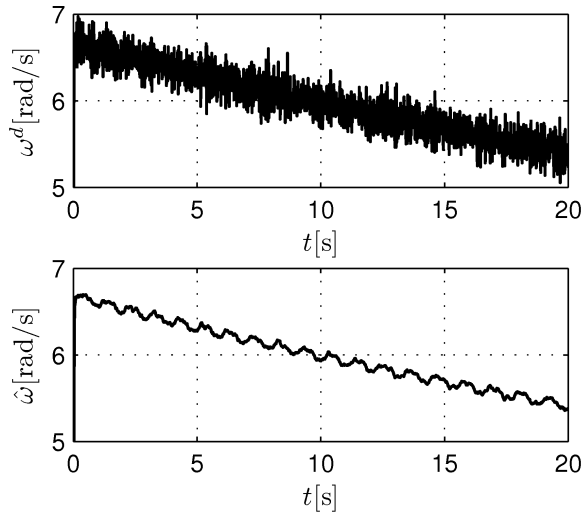

b) Estimates for lower velocity

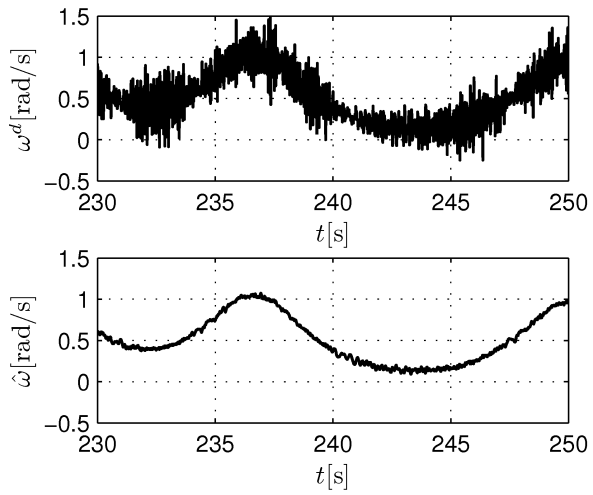

Fig. 8. Estimated velocity ω by difference estimator (ω^d) and EKF ($\widehat{\omega}$)

a) Estimates for higher velocity

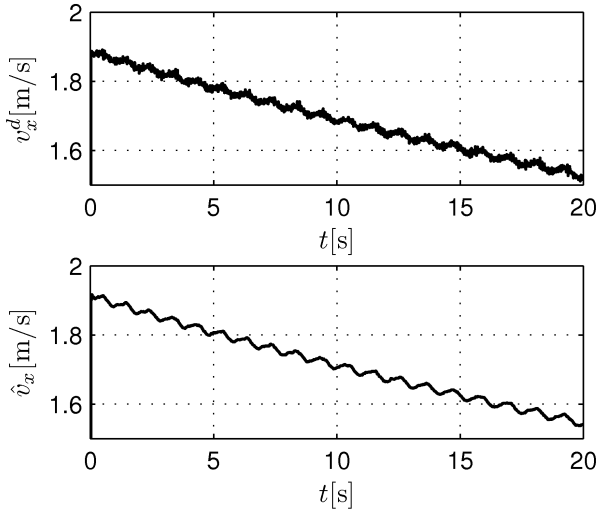

b) Estimates for lower velocity

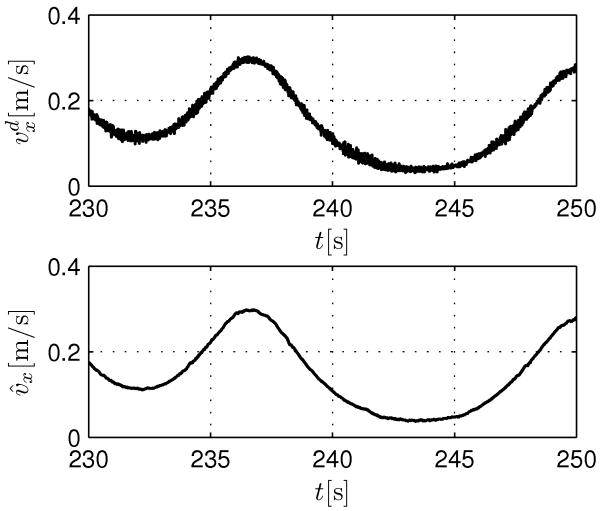

Fig. 9. Estimated velocity v_x by difference estimator (v_x^d) and EKF ($\widehat{v}_x$)

based on the difference estimator and EKF were compared. The advantage of the EKF is clear – the noise in velocity signal is significantly reduced. The instantaneous changes in velocity results from non stationary motion of the wheel – as a result of non zero gravitational torque velocity significantly fluctuates (in particular this can be observed for low velocities when kinetic energy of the wheel becomes small).

The estimation of accelerations also gives relatively good results. In Fig. 10 one can see that the noise is not predominant over a pure acceleration signal. A better result is quite difficult to achieve without affecting the resultant bandwidth of the measurement system.

a) Estimate of angular acceleration

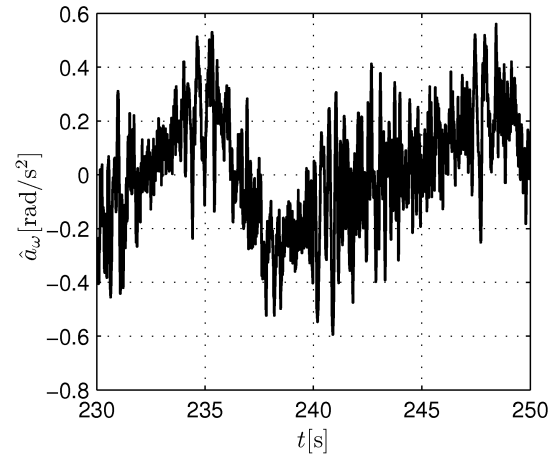

b) Estimate of linear acceleration

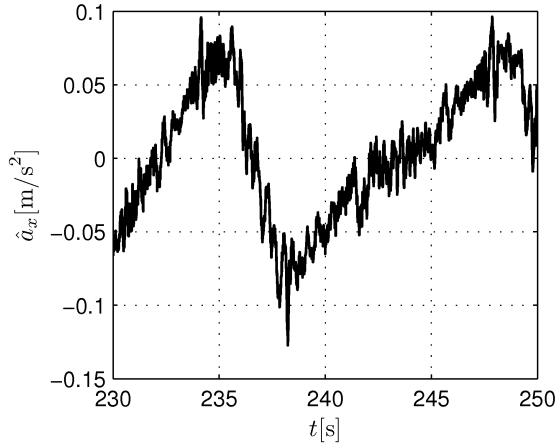

Fig. 10. Estimated accelerations

4.4. Example of application. Control algorithm description. In order to illustrate the usefulness of the overall measurement system velocity tracking the control problem for the wheeled skid-steering mobile robot (SSMR) is investigated. The SSMR is an an example of underactuated mechanical system with nonintegrable lateral dynamics [4]. Here we take into account a typical mechanical structure of the four-wheel driving mechanism, namely each pair of wheels with the same radius on the left and right side of the vehicle is mechanically coupled, as shown in Fig. 12. Hence, one can use angular velocities of left and right wheels as the following kinematic control input

$$\boldsymbol{u}_\omega \triangleq [\omega_L \ \omega_R]^T \in \mathbb{R}^2. \tag{22}$$

The control problem considered in this Sec. can be formulated as follows:

[4]In this case the lateral velocity v_y is treated as a bounded disturbance and is not taken into account directly.

Problem 1. Assuming that $v_{xr}(t)$ and $\omega_r(t)$ are bounded and time continuous reference velocities of the robot's body find bounded wheels velocities $\omega_L(t)$ and $\omega_R(t)$ such that the velocity tracking error

$$\tilde{\boldsymbol{\eta}}(t) \triangleq \begin{bmatrix} \omega(t) \\ v_x(t) \end{bmatrix} - \begin{bmatrix} \omega_r(t) \\ v_{xr}(t) \end{bmatrix} \tag{23}$$

satisfies

$$\lim_{t\to\infty} \|\tilde{\boldsymbol{\eta}}(t)\| \leq c, \tag{24}$$

for bounded slip/skid conditions, where $c > 0$ is a scalar constant.

Comparing the geometry of SSMR with respect to the geometry of the classical two-wheeled nonholonomic robot one can introduce the following virtual velocities ω^t and v^t

$$\begin{bmatrix} \omega^t & v_x^t \end{bmatrix}^T = \boldsymbol{P}\boldsymbol{u}_\omega, \tag{25}$$

where

$$\boldsymbol{P} \triangleq \begin{bmatrix} -\dfrac{r}{c} & \dfrac{r}{c} \\ \dfrac{r}{2} & \dfrac{r}{2} \end{bmatrix} \in \mathbb{R}^{2\times 2}, \tag{26}$$

with r and c denoting radius of the wheels and the distance between left and right wheels, respectively. In order to consider the additive slip disturbance one can introduce resulting angular and longitudinal slip functions

$$s^\omega \triangleq \frac{\omega^t - \omega}{\omega^t} \quad \text{and} \quad s^v \triangleq \frac{v^t - v_x}{v^t}. \tag{27}$$

Then measuring velocities ω, v_x, ω_L and ω_L one can calculate slip functions assuming that ω^t and $v^t \neq 0$. Additionally, in order to improve the slip estimation robustness to the measurement noise low-pass filtering, the dead zone and the saturation procedure are used. The discrete version of the algorithm with respect to the angular slip estimation is given as follows

S1 if $|\omega^t(n-1)| > \epsilon$ go to step S2, otherwise go to step S6
S2 calculate the current value of $\omega^t(n)$ from data coming from the measurement system based on Eq. (27)
S3 $s^\omega(n) := \dfrac{T_s}{T}\omega^t(n) + \left(1 - \dfrac{T_s}{T}\right) s^\omega(n-1)$
S4 if $s^\omega(n) > \overline{s}^\omega$ let $s^\omega(n) := \overline{s}^\omega$
S5 if $s^\omega(n) < \underline{s}^\omega$ let $s^\omega(n) := \underline{s}^\omega$
S6 $s^\omega(n-1) := s^\omega(n)$
S7 $\widehat{s}^\omega := s^\omega(n-1)$

For the proposed algorithm $\epsilon > 0$ is a constant, $T > 0$ denotes filter constant, T_s is the sample time, n determines number of sample and $\overline{s}^\omega$ and $\underline{s}^\omega$ are assumed upper and lower bounds of $\widehat{s}^\omega$, respectively. Initially one can assume $s^\omega(n-1) := 0$. The slip function $\widehat{s}^v$ can be estimated in a similar way.

Now using slip estimates $\widehat{s}^\omega$ and $\widehat{s}^v$ the following control solution can be proposed:

Proposition 1. Assuming that slip functions are slow time-varying[5] and bounded such that $\widehat{s}^\omega$ and $\widehat{s}^v < 1$ the following kinematic control law

$$\boldsymbol{u}_\omega = \boldsymbol{P}^{-1} \begin{bmatrix} (1-\widehat{s}^\omega)^{-1}\,\omega_r \\ (1-\widehat{s}^v)^{-1}\,v_{xr} \end{bmatrix} \tag{28}$$

satisfies control objective given by relationship (24).

In practical implementation the wheels velocity $\boldsymbol{u}_\omega$ can be regarded as the desired input dependent on current estimates of slip for on-board motor controllers. The structure of the control system is presented in Fig. 11. The algorithm gives possibility to control motors with relatively high sampling rate[6] and significantly improved performance of the velocity tracking in the presence of the limited, bounded and slow-time varying wheel slip.

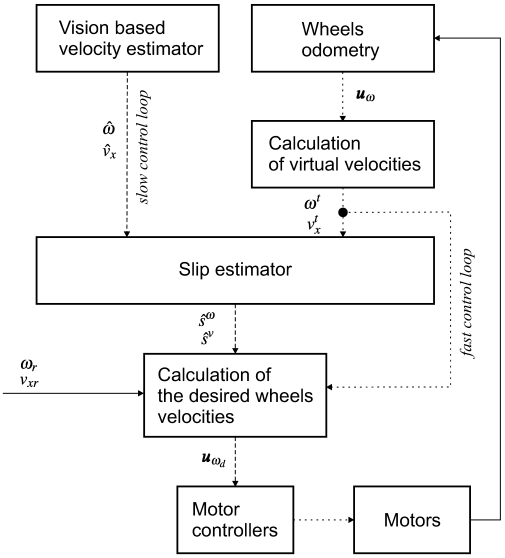

Fig. 11. Structure of the control system for SSMR with velocity and slip estimators

Experimental setup. During experiments the mobile robot platform MMS with the skid-steering four wheel drive [18] was used with the LED marker placed on it – see Fig. 12. The robot can exchange data with PC computer via the low-latency and fast radio module using the CC2400 chip connected to PC by the serial interface RS232 with the speed 115.2 kb/s. The onboard PID controllers with feedforward term are responsible for the accurate velocity control of the wheels and work with frequency 1 kHz. The high control feedback is realized with frequency 64 Hz and takes advantage of the described measurement system. Based on the algorithm given in this section slip functions are calculated by PC and then they are sent together with the desired angular ω_r and longitudinal v_r velocities to the robot controller. It is assumed that the filter constant $T = 0.15$ s and estimated slip functions must be in the interval $[-0.2,\ 0.7]$ in order to increase robustness of an estimation of lower velocities. The experiment was conducted for eight like shape trajectory given as

$$\begin{bmatrix} X_r(t) \\ Y_r(t) \end{bmatrix} = \begin{bmatrix} 0.25\sin(0.45t) \\ 0.25\sin(0.9t) \end{bmatrix}, \tag{29}$$

[5]This assumption can be justified especially for the steady-state slip condition.
[6]It can be easily realized, for example, using high resolution incremental encoders in order to measure wheels velocities.

where t denotes time. The reference orientation is calculated based on unicycle-like kinematics and satisfies

$$\theta_r = \operatorname{atan2}\left(\dot{Y}_r, \dot{X}_r\right). \tag{30}$$

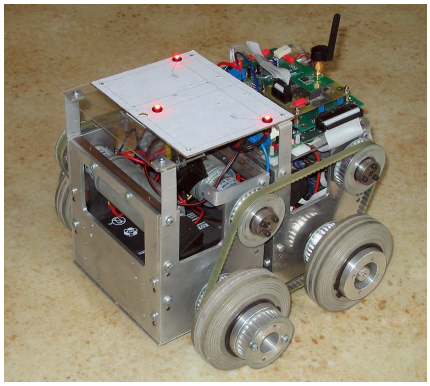

Fig. 12. Experimental mobile robot SSMR MMS with the marker

In spite of that reference coordinates are not taken into account during control (only slip compensation is considered) they are used for reference velocity calculations. For simplicity the lateral velocity is not considered (it cannot be compensated since according to [19] it is an unmatched perturbation). In turn angular and linear velocities satisfy

$$\omega_r \triangleq \dot{\theta}_r \quad \text{and} \quad v_r \triangleq \cos\theta_r \dot{X}_r + \sin\theta_r \dot{Y}_r. \tag{31}$$

The experiments were conducted for two cases. For the first case, no slip compensation was used, namely the robot's velocity was estimated based on relationship (25). As one can see from Fig. 13 the velocity tracking is not accurate. In particular (see Fig. 13a) the angular velocity ω does not correspond to the desire signal ω_r in the range of higher values when a significant slip appears. The error tracking for the longitudinal velocity is smaller – see Fig. 13b. Comparing Figs. 13c and 13a) one can conclude that the lateral velocity components v_y appears when magnitudes of ω increase [20]. As a result of not accurate velocity tracking, the resultant path of the robot is far from the theoretical path as can be seen from Fig. 13d. Hence, the localization method based on odometry for SSMR is highly limited.

a) Angular velocity: estimated $\widehat{\omega}$ (–) and desired ω_r (– –)

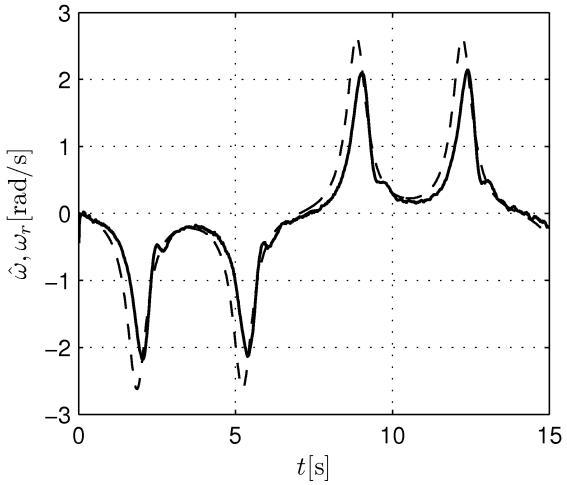

b) Longitudinal velocity: estimated $\widehat{v}_x$ (–) and desired v_r (– –)

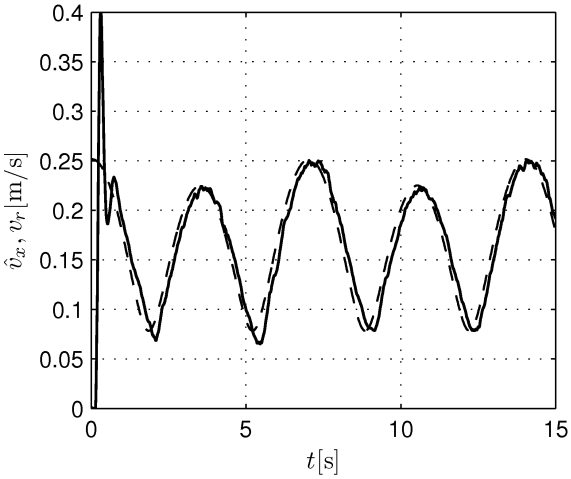

c) Estimated lateral velocity $\widehat{v}_y$

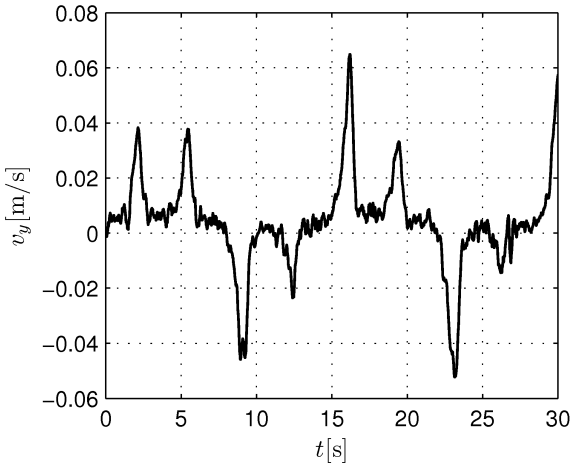

d) Reference (– –) and obtained position path (–)

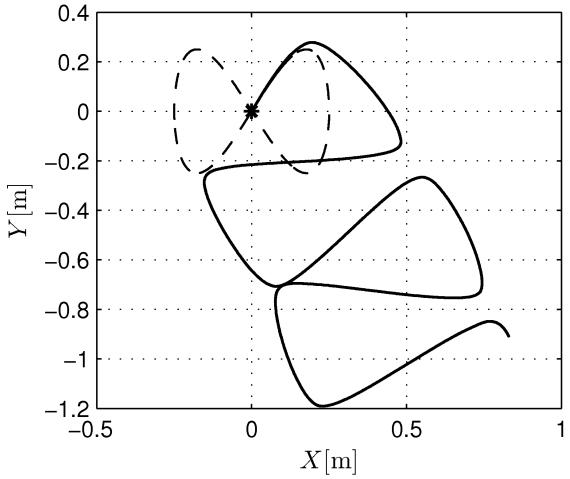

Fig. 13. Velocity tracking without slip observer using the described measurement and control system

Using a slip compensation gives possibility to significantly improve the control performance and the velocity tracking accuracy. Such evident improvements can be observed from Figs. 14a and 14b in particular with respect to the angular velocity. The time plot of lateral velocity presented in Fig. 14c shows that magnitude of v_y does not exceed 0.06 m/s. As

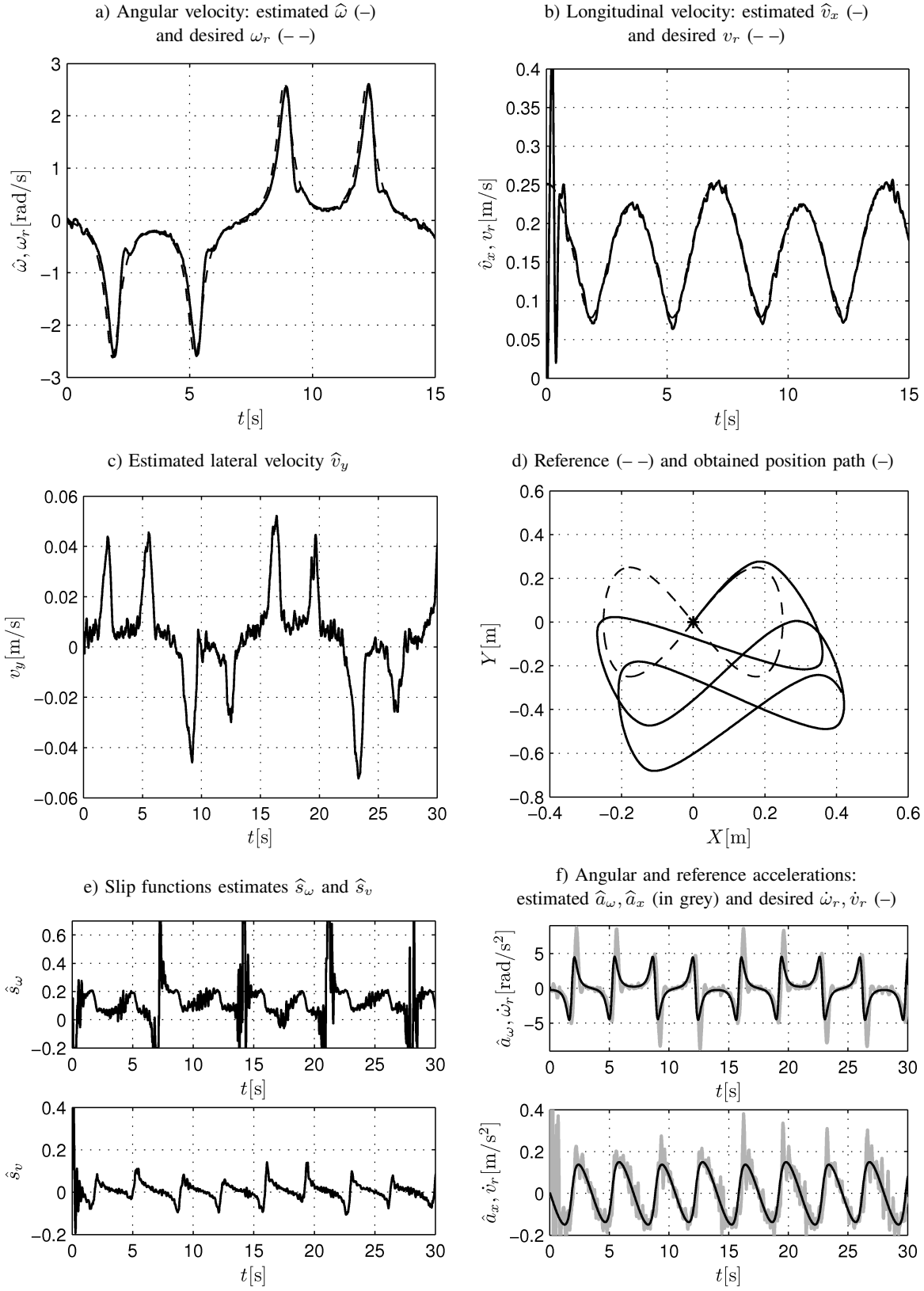

Fig. 14. Velocity tracking with slip observer using the described measurement and control system

a result of more accurate velocity tracking the path of the robot becomes closer to the reference path as illustrated in Fig. 14d. The slip functions are presented in Fig. 14e – their values fluctuate rapidly in the range of low velocities (therefore they are saturated). The angular slip is significantly higher but its average does not exceed 0.2. Additionally, in Fig. 14f estimated accelerations are compared with reference ones. As one can see, the quality of the acceleration estimation provided by the described measurement system gives astonishingly good results.

To get the quantitative comparison of experimental results, the following integral performance indexes were calculated

$$I_\omega \triangleq \frac{1}{T_H}\sqrt{\int_0^{T_H} \left(\omega\left(t\right)-\omega_r\left(t\right)\right)^2 dt} \tag{32}$$

and

$$I_{vx} \triangleq \frac{1}{T_H}\sqrt{\int_0^{T_H} \left(v_x\left(t\right)-v_r\left(t\right)\right)^2 dt}, \tag{33}$$

where T_H denotes time horizon. For $T_H = 30$ s using slip compensation the integral performance indexes are decreased from

$$I_\omega = 0.0676 \quad \text{and} \quad I_{vx} = 0.0048$$

to

$$I_\omega = 0.0325 \quad \text{and} \quad I_{vx} = 0.004,$$

respectively.

5. Concluding remarks

In this paper the localization system based on vision system taking advantage of the subpixel image analysis is described. It is designed for the robot posture measurement as well as for velocity and acceleration estimation in the case of the planar motion. Conducted experiments show good quality of the position and orientation measurement which are the base for the accurate estimation of velocity and acceleration. Usefulness of the localization system with Kalman estimator is illustrated by the example application for the control problem of the skid-steering mobile robot. In this case some data fusion, based on the odometry and vision subsystems working with different frequencies, were also proposed for skid/slip compensation. Although the accuracy of the measurement system is indeed satisfactory we believe that using faster CCD sensor and the real-time operating system it is possible to obtain even better results in control.

Moreover, one can improve the overall sensor system by using additional inertial sensors in the form of accelerometers and gyros mounted on the robot's chassis (cf. [21]). In particular it should improve the bandwidth of the observer which is critical for the control application. The main drawback of this solution is an increase of technical and computational requirements (for example the algorithm should be calculated by real-time system like DSP, bias of the sensors should be taken into account in the process model).

The presented algorithms can be implemented with a camera placed on the moving vehicle. Such a solution gives possibility to extend scope of the localization system also in the real environment, however, finally it may lead to more complicated and less accurate measurement system.

REFERENCES

[1] I. Dulęba, *Algorithms of Motion Planning for Nonholonomic Robots*, Wrocław University of Technology Publishing House, Wrocław, 1998.

[2] S.M. LaValle, *Planning Algorithms*, Cambridge University Press, Cambridge, 2006.

[3] H.R. Everett, *Sensors for Mobile Robots: Theory and Application*, AK Peters, Wellesley, Massachusetts, 1995.

[4] E. Bayro-Corrochano, L.E. Falcon-Morales, and J. Zamora-Esquivel, "Visually guided robotics using conformal geometric computing", in *Mobile Robots, Perception & Navigation*, pp. 19–44, ed. S. Kolski, Pro Literatur Verlag, Mammendorf, 2007.

[5] P. Skrzypczyński, *Methods of Analysis and Uncertainty Perception Reduction in Navigation System of Mobile Robot*, Thesis No. 407, Poznań University Publishing House, Poznań, 2007, (in Polish).

[6] T. Cheviron, T. Hamel, R. Mahony, and G. Baldwin, "Robust nonlinear fusion of inertial and visual data for position, velocity and attitude estimation of UAV", *IEEE Int. Conf. on Robotics and Automation* 7, 2010–2016 (2007).

[7] K. Kozlowski and D. Pazderski, "Stabilization of two-wheeled mobile robot using smooth control laws – experimental study", *Proc. IEEE Int. Conf. on Robotics and Automation* 9, 3387–3392 (2006).

[8] W.E. Dixon, D.M. Dawson, E. Zergeroglu, and A. Behal, "Adaptive tracking control of a wheeled mobile robot via an uncalibrated camera system", *IEEE Transactions on Systems, Man, and Cybernetics* 31 (3), 341–362 (2001).

[9] D. Pazderski, *Control of Some Class of Nonholonomic Systems Using Kinematic Oscillator*, PhD thesis, Poznań University of Technology, Poznań, 2007, (in Polish).

[10] P. Dutkiewicz, M. Kiełczewski, and M. Kowalski, "A tracking vision system of mobile robots", *Conf. Volume Lightmetry 02: Metrology and Testing Techniques Using Light* 2, 319–327 (2002).

[11] J. Heikkilä and O. Silvén, "A four-step camera calibration procedure with implicit image correction", *Proc. IEEE Computer Society Conference on Computer Vision and Pattern Recognition* 5, 1106–1112 (1997).

[12] R.Y. Tsai, "A versatile camera calibration technique for high accuracy 3D machine vision metrology using off-the-shelf TV cameras and lenses", *IEEE J. Robotics and Automation* RA-3 (4), 323–344 (1987).

[13] J.Y. Bouguet, *Camera Calibration Toolbox for Matlab*, http://www.vision.caltech.edu/bouguetj/calib_doc/ (2007).

[14] P. Kulczycki, "Applicational possibilities of nonparametric estimation of distribution density for control engineering, *Bull. Pol. Ac.: Tech.* 56 (4), 347–359 (2008).

[15] A. Levant, "Robust exact differentiation via sliding mode technique, *Automatica* 34, 379–384 (1998).

[16] G. Welch and G. Bishop, *An Introduction to the Kalman Filter*, TR 95-041, UNC-Chapel Hill, USA, 2002.

[17] D. Simon, *Optimal State Estimation: Kalman, H Infinity, and Nonlinear Approaches*, Wiley-Interscience, London, 2006.

[18] D. Pazderski and K. Kozlowski, "Trajectory tracking control of skid-steering robot – experimental validation", *Proc. Triennial Event of International Federation of Automatic Control* 1, CD-ROM (2008).

[19] C.B. Low and D. Wang, "Modeling and analysis of skidding and slipping in wheeled mobile robots: control design perspective", *IEEE Transactions on Robotics* 24 (3), 676–687 (2008).

[20] K. Kozłowski and D. Pazderski, "Practical stabilization of a skid-steering mobile robot: A kinematic-based approach", *IEEE Int. Conf. on Mechatronics* 2, 519–524 (2006).

[21] Jingang Yi, Hongpeng Wang, Junjie Zhang, Dezhen Song, S. Jayasuriya, and Jingtai Liu, "Kinematic modeling and analysis of skid-steered mobile robots with applications to low-cost inertial-measurement-unit-based motion estimation", *IEEE Transactions on Robotics* 31 (3), 1087–1097 (2009).